Original Article

Effect of initial coating crack on the mechanical performance of surface-coated zircaloy cladding

Ze Xu [a], Yulan Liu [a, *], Biao Wang [b]

[a] Department of Applied Mechanics and Engineering, Sun Yat-Sen University, Guangzhou, 510000, China
[b] Sino-French Institute of Nuclear Engineering and Technology, Sun Yat-Sen University, Zhuhai, 519082, China

ABSTRACT

In this paper, the mechanical performance of cracked surface-coated Zircaloy cladding, which has different coating materials, coating thicknesses and initial crack lengths, has been investigated. By analyzing the stress field near the crack tip, the safety zone range of initial crack length has been decided. In order to determine whether the crack can propagate along the radial (r) or axial (z) directions, the energy release rate has been calculated. By comparing the energy release rate with fracture toughness of materials, we can divide the initial crack lengths into three zones: safety zone, discussion zone and danger zone. The results show that Cr is suitable coating material for the cladding with a thin coating while Fe−Cr−Al have a better fracture mechanical performance in the cladding with thick coating. The Si-coated and SiC-coated claddings are suitable for reactors with low power fuel elements. Conclusions in this paper can provide reference and guidance for the cladding design of nuclear fuel elements.

© 2020 Korean Nuclear Society, Published by Elsevier Korea LLC. This is an open access article under the CC BY-NC-ND license (http://creativecommons.org/licenses/by-nc-nd/4.0/).

1. Introduction

In order to improve the quality of the environment, clean energy is playing an increasingly role in the world. Nuclear energy is an important type of clean energy. Because it has high efficiency, environmental protection and other properties that traditional energy cannot be compared. However, the use of nuclear energy has certain safety risks. Ensuring the safe operation of nuclear reactors has been widely concerned, especially after the accident of Fukushima nuclear power plant.

The cladding plays a key role in the fuel rod. It ensures the separation of fuel pellets from the coolant. That is, it prevents fission products from leaking out of fuel rods and ensures that the coolant does not penetrate into fuel rods. Also, excellent mechanical properties of the cladding are essential, such as strength, stiffness, thermal conductivity and corrosion resistance. Therefore, investigation on the fuel cladding is nonnegligible.

Zirconium alloy is traditionally and commonly used as the cladding material. However, with the increasing demands for cladding, such as lower oxidation resistance, stronger mechanical properties and better heat transfer performances, an alternative type of cladding

should be investigated. At present, several new types of cladding have been researched. These include surface-coated Zircaloy, full SiC_f/SiC and Ti_3SiC_2 [1]. Compared with other claddings, an irreplaceable advantage of the surface-coated Zircaloy cladding is that no brand new investigation is required. The reason is that it can be investigated based on the previous studies on pure Zircaloy cladding. Therefore, the surface-coated Zircaloy cladding can be seen as a near-term choice for the fuel element [2].

Some numerical simulation analyses have been used to study performances of the surface-coated Zircaloy cladding. According to MELCOR systems code, which has been validated by experimental results, reference [3] found that the coating could reduce the initial rate of hydrogen generation, which could decrease the rate of cladding oxidation. References [4,5] calculated the stress distribution in the cladding with different coating. Pressure difference, thermal expansion, irradiation-induced axial growth and creep were considered in their investigation. Also, experimental analyses are certainly used. Reference [6] did a long-term corrosion test and observed the performance of multicomponent fuel cladding. References [7,8] investigated the radiation response of surface-coated Zircaloy-4 cladding which was coated by FeCrAl. It found FeCrAl-coated Zircaloy-4 cladding performed better than the cladding which had no coating materials at irradiation response performance, especially in terms of oxidation resistance. According to experiments, reference [9] investigated the adhesion property and high-temperature oxidation

behavior of surface-coated Zircaloy cladding. It found that there were high adhesion and no relative slip between cladding and coating. That is, detachment of coating cannot happen unless the stress level in the cladding is large enough. However, this stress level is large enough to destroy the materials of cladding, and coating failure is caused by material failure rather than crack propagation. Therefore, the coating peeling is not concerned in this paper.

Influence of material properties were mainly focused in these previous investigations. However, cracks, even fracture, were certainly observed in experiments [9]. That means the coating failure may occur because of the internal cracks rather than the failure of material itself. So it is important to investigate performances of coating material with cracks. Reference [10] analyzed cracks of Cr-coated cladding by numerical simulation and reference [11] found the damage mechanisms of Cr-coated cladding by experiment. In this paper, a model of surface-coated Zircaloy cladding with initial crack in the coating was created to analyze. According to theoretical analysis method, mechanical behaviors of the coating under the normal operation, such as stress, stress intensity factor, energy release rate were concerned. Conditions for crack propagation and coating failure were calculated. A previous study [12] has shown that the coating of the cladding should contain at least one of the following materials, Cr, Al and Si. Therefore, in order to find the optimal design of surface-coated Zircaloy cladding, different materials of coating were considered. In actual nuclear engineering, pure aluminum is not used as the coating material because of its low intensity. However, aluminum alloys, such as Fe—Cr—Al, are widely used in the coating. Furthermore, the ceramic material, SiC, is also a hot topic in the investigation of surface-coated cladding. Therefore, four coating materials, Cr, Si, SiC, Fe—Cr—Al were investigated in this paper.

2. Model and method

The theoretical analysis of fracture mechanics was used in our investigation. The reason is that the cost of experiments of crack propagation in surface-coated Zircaloy cladding is huge. Because the number of samples needed for experiments is large. Meanwhile, these samples are difficult to manufacture because the initial crack length in the coating is small. Based on the theoretical analysis, the stress distribution and crack propagation in the coating can be investigated qualitatively and quantitatively. Meanwhile, the results can be used as reference for future experiments. The total analysis contained four steps: 1) calculating the stress distribution in the coating, 2) using results in step one to calculate the stress distribution near crack tip, 3) analyzing conditions for crack propagation and coating failure in different initial crack length and coating thickness, 4) comparing fracture properties of different coating materials. The steps 2—4 were important investigation in this paper.

2.1. Stress distribution in the coating

The stress distribution was calculated based on the previous investigation [13]. In Lee's study, just stress distribution in multilayered SiC cladding was investigated. But the analysis method was also applicable to the surface-coated Zircaloy cladding. We gave a brief introduction to the analysis method here. Considering the axial symmetry of the fuel rod, a simplified model was used, as shown in Fig. 1.

The bottom of the fuel rod was constrained and axial dimension (z-direction) was much larger than other directions (r-direction and θ-direction). Therefore, it can be seen as a plane strain problem that the displacement along the z-direction is zero. Boundary conditions were established by referencing to typical values for PWR [14]. The
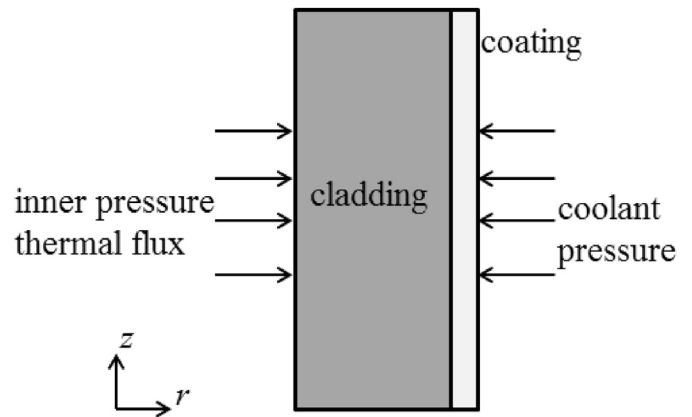

Fig. 1. The axisymmetric model and its boundary conditions.

coolant pressure was constant of 15.5 MPa. Inner pressures contained the gas pressure, which was constant, and the contact pressure between fuel pellets and the cladding. The contact pressure and thermal flux vary with time at the beginning of the operation. With the increase of burnup, they approach a constant. To simplified calculation, the whole inner pressure was established at 20 MPa and the uniform power generation by fuel pellets was 20 kW/m, which were close to values under the normal operation.

Considering energy conservation equations, mechanical equilibrium equations, geometrical equations and constitutive equations, the stress distribution in cladding and coating can be obtained. The expression of the stress distribution in three principle directions is complicated. In this paper, we focus on the hoop stress distribution in the coating. The reasons are: 1. Compared with the hoop and axial stress, the radial stress can be ignored based on Lee's study. 2. The crack propagates along the radial direction. The crack propagation in the plane of crack is perpendicular to the circular direction and relies on hoop stress. The axial stress is perpendicular to the plane of crack, so it has little contribution to the crack propagation. 3. Because of the stress concentration caused by hoop stress, the stress distribution near the crack tip is mainly determined by hoop stress rather than axial stress. The axial stress does affect the stress distribution far from the crack tip, but the stress level far from the crack tip is lower than the ultimate strength of material. Therefore, we just gave the formula that described the hoop stress distribution [4,13]:

$$
\begin{aligned}
\sigma_\theta = {}& \frac{E}{(1-\nu)r^2}\int_{r_i}^{r_o} Gr\,\mathrm{d}r - \frac{GE}{1-\nu} - \frac{E\xi}{(1+\nu)r^2}\int_{r_i}^{r_o} r\ln(r)\,\mathrm{d}r \\
& - \frac{\nu E\xi\ln(r)}{(1+\nu)(1-2\nu)} - \frac{(1-\nu)E\xi}{(1+\nu)(1-2\nu)} \\
& + \frac{E}{1+\nu}\left(\frac{C_1}{1-2\nu} + \frac{C_2}{r^2} + \frac{\nu\varepsilon_0}{1-2\nu}\right)
\end{aligned}
\tag{1}
$$

Where σ_θ is hoop stress (Pa), E is Young's modulus (Pa), ν is Poisson's ratio $(-)$, r_o and r_i are outer and inner radius of the cladding, ε_0 is initial strain $(-)$, C_1 and C_2 are constants which are calculated by boundary conditions, G and ξ are intermediate variables which are described by the following formula:

$$\begin{cases} G = \dfrac{\nu K_2 + (1-\nu)K_1}{(1+\nu)} \\[2mm] \xi = \dfrac{[(1-2\nu)K_2 + (2\nu-1)K_1]}{(1-\nu)} \\[2mm] K_1 = \varepsilon_{C,r} + \nu\left[\varepsilon_{C,z} + \left(\dfrac{\Delta L}{L}\right)_i\right] \\[2mm] K_2 = \varepsilon_{C,\theta} + \nu\left[\varepsilon_{C,z} + \left(\dfrac{\Delta L}{L}\right)_i\right] \end{cases} \quad (2)$$

Where $\varepsilon_{C,r}$, $\varepsilon_{C,\theta}$ and $\varepsilon_{C,z}$ are strain induced by creep in different principle directions (−), respectively. $\left(\frac{\Delta L}{L}\right)_i$ is irradiation axial growth (−).

Equations (1) and (2) describe the stress distribution under creep. In order to obtain the thermal stress distribution, the creep strain term in constitutive equations should be changed into the thermal strain term and be calculated once again [4,13].

The hoop stress distribution relies on the material properties. Some thermal mechanical properties of Zr, Cr, Si, SiC and Fe−Cr−Al, which are investigated in this paper, are summarized in Table 1.

In general, material properties vary with temperature. However, under the normal operation, the temperature of the cladding and coating changes little because of their high thermal conductivities. Therefore, material properties at coolant temperature (500 K) were used to calculate the stress distribution.

2.2. Stress distribution near crack tip

Under the normal operation, because of the singularity of the crack tip, the stress concentration must occur near the crack tip. If the stress concentration zone extends to the cladding, cracks may develop and propagate in the cladding. It may cause the coolant to enter the inside of the cladding and fission products to spread out. The cladding failure occurs in the end. Therefore, it is important to obtain the stress distribution near the crack tip.

The radial and axial dimensions of the coating differ greatly. For PWR, the usual used radial dimension is between 10 μm and 100 μm while the axial dimension is at least 10 cm. Therefore, it can be seen as a plane strain problem, as shown in Fig. 2. The usual thickness of the cladding is 0.57 mm [27]. In order to ensure the simply and uniformly manufacturing of fuel elements, the thickness of cladding cannot be changed. Therefore, just the thickness of coating varies in actual engineering. The thickness of coating varied from 10 μm to 100 μm in our investigation. If the coating is too thin, the production will be more difficult and the cost will increase. If the coating is too thick, the surface-coated zircaloy cladding will become multi-layered cladding, which is not the main research object in this investigation.

Compared with the circumference of coating, the initial crack length is small enough. Therefore, it can be seen from the right region in Fig. 2 that the curvature of the coating was not be considered during the calculation of the stress distribution. This
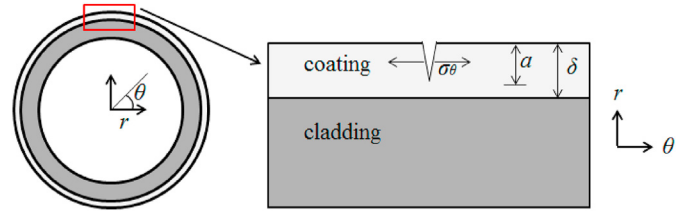

Fig. 2. The vertical view of the cladding and coating (left) and enlarged view of the initial crack (right).

hypothesis has little effect on results but the computing efficiency can improve significantly. Also, the crack propagation is mainly related to the hoop stress. The initial crack formed in the coating is opening mode crack (Mode I). The stress distribution can be described by the following formula [28]:

$$\begin{cases} \sigma_{\tilde{r}} = \dfrac{K_I}{\sqrt{2\pi\tilde{r}}}\cos\dfrac{\tilde{\theta}}{2}\left(1 - \sin\dfrac{\tilde{\theta}}{2}\sin\dfrac{3\tilde{\theta}}{2}\right) \\[2mm] \sigma_{\tilde{\theta}} = \dfrac{K_I}{\sqrt{2\pi\tilde{r}}}\cos\dfrac{\tilde{\theta}}{2}\left(1 + \sin\dfrac{\tilde{\theta}}{2}\sin\dfrac{3\tilde{\theta}}{2}\right) \\[2mm] \sigma_{\tilde{z}} = \nu(\sigma_{\tilde{r}} + \sigma_{\tilde{\theta}}) \\[2mm] \tau_{\tilde{r}\tilde{\theta}} = \dfrac{K_I}{\sqrt{2\pi\tilde{r}}}\cos\dfrac{\tilde{\theta}}{2}\sin\dfrac{\tilde{\theta}}{2}\cos\dfrac{3\tilde{\theta}}{2} \\[2mm] \tau_{\tilde{r}\tilde{z}} = \tau_{\tilde{\theta}\tilde{z}} = 0 \end{cases} \quad (3)$$

Where $\sigma_{\tilde{r}}$, $\sigma_{\tilde{\theta}}$, $\sigma_{\tilde{z}}$, $\tau_{\tilde{r}\tilde{\theta}}$, $\tau_{\tilde{r}\tilde{z}}$ and $\tau_{\tilde{\theta}\tilde{z}}$ are normal stress and shear stress in different directions (Pa), respectively, K_I is opening mode crack stress intensity factor (N·m$^{-3/2}$), $\tilde{r}$, $\tilde{\theta}$ and $\tilde{z}$ are three directions in the coordinate system, which the crack tip is the coordinate origin, as shown in Fig. 3 ($\tilde{z}$ is the same as z in Fig. 1.).

The stress intensity factor relies on the geometry and boundary conditions of the coating. In our investigation, the coating is bonded to the cladding. The coating was chosen as the object of investigation. The effect of the bonding between coating and cladding was considered as the force acting on the coating. Therefore, stress states of the coating with initial crack are coolant pressure (radial direction), the effect of bonding (radial direction and hoop direction) and internal stresses of the coating. The radial component of the effect of bonding is in balance with the coolant
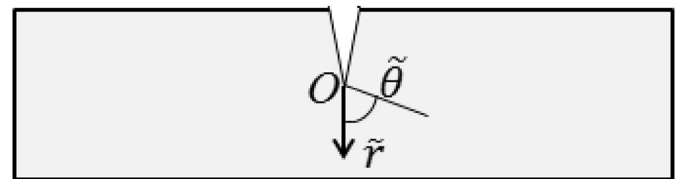

Fig. 3. The coordinate system during calculations of the stress distribution near crack tip.

Table 1
Thermal mechanical properties of cladding and coating materials (the temperature is 500 K).

	Zr	Cr	Si	SiC	Fe−Cr−Al
Young's modulus (GPa)	68 [15]	280 [16]	169 [17]	460 [18]	205 [19]
Poisson's ratio (−)	0.3 [15]	0.22 [16]	0.23 [17]	0.21 [18]	0.3 [19]
Thermal expansion coefficient (1/K)	6.5×10^{-6} [4]	9.1×10^{-6} [20]	2.6×10^{-6} [21]	4.7×10^{-6} [18]	12×10^{-6} [19]
Thermal conductivity (W/mK)	16.4 [4]	76 [20]	28 [21]	9.5 [18]	16 [19]
Fracture toughness (kJ/m^2)	/	0.1−0.3 [22]	0.0064−0.0072 [23]	0.012−0.054 [24,25]	0.21−0.31 [26]

pressure and the hoop component is approximately equal to σ_θ in the coating. The coolant has a low probability to enter the crack if the crack cannot propagate. The reasons are: 1) the initial crack in the coating is tiny, 2) the initial crack opening displacement is small. Therefore, only σ_θ, rather than the coolant pressure on the crack, is considered in the calculating of the stress intensity factor. And the stress intensity factor can be calculated by the following formula [29]:

$$K_{\mathrm{I}} = \sigma_\theta \sqrt{a}\left[1.99 - 0.4\left(\frac{a}{\delta}\right) + 18.7\left(\frac{a}{\delta}\right)^2 - 38.48\left(\frac{a}{\delta}\right)^3 + 53.85\left(\frac{a}{\delta}\right)^4\right]$$

(4)

a and δ are crack length and thickness of the coating (m) in Fig. 2.

It is complex to compare three normal stresses and shear stresses of different materials and crack lengths. Therefore, the von Mises stress was calculated to describe the stress level of the crack tip. As shown in equation (5).

$$\sigma_{\mathrm{m}} = \frac{1}{\sqrt{2}}\sqrt{(\sigma_{\bar{r}} - \sigma_{\bar{\theta}})^2 + (\sigma_{\bar{\theta}} - \sigma_{\bar{z}})^2 + (\sigma_{\bar{z}} - \sigma_{\bar{r}})^2 + 6(\tau_{\bar{r}\theta}^2 + \tau_{\theta\bar{z}}^2 + \tau_{\bar{z}\bar{r}}^2)}$$

(5)

Where σ_{m} is the von Mises stress (Pa).

2.3. Crack propagation and coating failure

As shown in Fig. 4, the initial crack in the coating may propagate along two directions, r-direction and z-direction. According to the superposition principle, these propagations can be viewed as two processes. First, the crack propagates along r-direction until the limit length of crack propagation. Second, the crack propagates along z-direction. However, if the crack can propagate to the cladding region, the cladding failure will happen and the propagation along z-direction is not important. Therefore, if the crack can propagate along r-direction to the cladding, the propagation along z-direction will not be discussed in this paper.

The crack propagation relies on the relation between energy release rate and fracture toughness of materials. It can be described as:

$$\begin{cases} \text{the crack can propagate}, & G > \Gamma \\ \text{the crack cannot propagate}, & G \le \Gamma \end{cases}$$

(6)

Where G is energy release rate (kJ/m²), Γ is fracture toughness which represents the energy release rate at critical crack propagation (kJ/m²).

Because of the difference between the radial and axial dimensions, the energy release rate need to be calculated in different methods. When the crack propagates along r-direction, it can reach the cladding region after a short distance of propagation. The energy release rate can be calculated by the opening mode crack stress intensity factor which has been calculated in 2.2:

$$G_r = \frac{K_{\mathrm{I}}^2(1 - \nu^2)}{E}$$

(7)

Where G_r is energy release rate when the crack propagates along r-direction (kJ/m²).

When the crack propagates along z-direction, a crack channel will be formed in the coating. If the energy release rate is large enough, the crack can keep propagating until the coating is penetrated by the crack. The energy release rate can be calculated by the following formula [30]:

$$G_z = \frac{\sigma_\theta^2 \pi \delta (1 - \nu^2)}{2E} g(\alpha, \beta)$$

(8)

Where G_z is energy release rate when the crack propagates along z-direction (kJ/m²), α and β are functions of materials of coating and cladding, $g(\alpha, \beta)$, which can be obtained by looking up the parameters table, is a function of α and β. The specific data is shown in Table 2.

3. Results and analysis

The coating is much thinner than the cladding, so the hoop stress distribution in the coating is approximately a constant. This hypothesis can improve the computing efficiency but have no significant effect on results. Because there are many variables in the investigation, such as coating thickness, initial crack length, coating material, it is not possible and necessary to put all results in the paper. Therefore, in this section, we selected representative results for interpretation and analysis. Other results are also consistent with conclusions in this investigation.

3.1. Crack tip stress analysis

Fig. 5 shows the von Mises stress distribution near the crack tip. The coating material is Cr, and the coating thickness and initial crack length are 100 μm and 50 μm, respectively.

The von Mises stress near the crack tip reached the GPa level, which is much larger than ultimate strength of the material. The crack in the coating may propagate in order to release the high strain energy. In the region far from the crack tip, the von Mises stress drops sharply to a normal level (MPa). In order to observe the relation between the von Mises stress and the distance from the crack tip more intuitively, we gave a two-dimensional image of Fig. 6. With the increase of the radial distance from the crack tip, the stress level in the coating went through three stages. From 0 μm to about 4 μm, the von Mises stress level reached several GPa, which is much more than ultimate strength of the cladding material, and decreased sharply. This area is called "the danger zone". From 4 μm to about 17 μm, the von Mises stress level droped gently and the value did not exceed ultimate strength of the cladding material. This area is called "the transition zone". From 17 μm to the interface
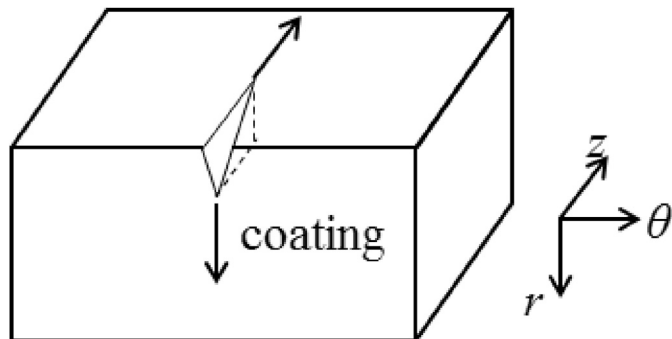

Fig. 4. Two modes of crack propagation: radial propagation and axial propagation.

Table 2
Calculation parameters of different coating materials in equation (8) [31,32].

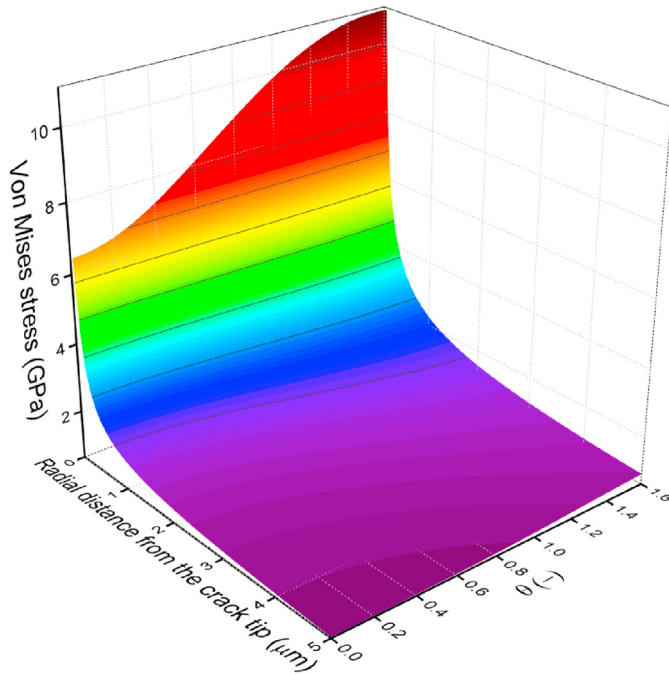| Coating material	Cr	Si	SiC	Fe−Cr−Al
α	0.59	0.41	0.73	0.50
β	0.16	0.10	0.20	0.14
$g(\alpha, \beta)$	2.34	1.83	3.02	2.05

Fig. 5. Von Mises stress distribution near the crack tip.
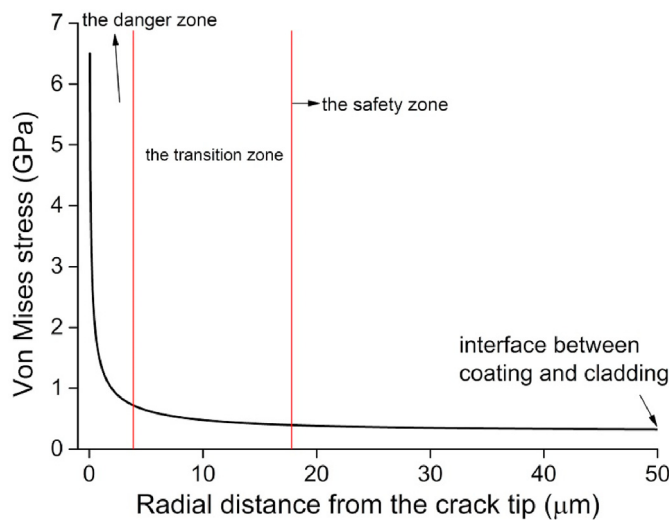

Fig. 6. Von Mises stress distribution along the radial direction.

between coating and cladding, there was little change in the von Mises stress level and the value was approximately equal to the hoop stress in the cladding. This area is called "the safety zone". Other situations which have different coating materials, coating thicknesses and initial crack lengths had the same conclusions as Figs. 5 and 6 while there were just some differences in stress values and the range of three zones. It is important to ensure the zone in which the interface between coating and cladding is located. If it is located in the transition or safety zone, the cladding will not affected by the stress concentration near the crack tip. However, if it is located in the danger zone, the stress level is higher than the uliminate strength of cladding and cracks can develop and propagate in the cladding. Therefore, the von Mises stress at the interface between coating and cladding has been described, as shown in Fig. 7:

We just described the von Mises stress at four different coating thicknesses. Other results showed the similar trend to results in Fig. 7. For the same coating thickness, SiC-coated cladding had the highest stress level at the interface between coating and cladding while the stress level of the other three materials did not differ significantly. This is caused by the greatly difference between the Young's modulus of Zr and SiC. Because of the high adhesion, there was no relative sliding between the coating and cladding. Therefore, the coating and cladding had the same deformation at the interface. A small stress changing in the material which has high Young's modulus could result in a large stress changing in the material which has low Young's modulus. Therefore, choosing right materials of coating and cladding plays an important role in reducing the von Mises stress level.

For the same coating material, the maximum von Mises stress at the interface increased with the coating thickness. Considering that the ultimate strength of Zr is about 650 MPa [19], we can obtain the critical crack length when the von Mises stress in the cladding reaches the ultimate strength, as shown in Fig. 8:

It can be seen from Fig. 8 that the critical crack length of different coating materials approximately linear with the coating thickness. That is, for the same material, the ratio of critical crack length and coating thickness is approximately a constant. Therefore, if we confirm the coating thickness, the maximum allowable crack length in the coating is determined accordingly. The ratio of Cr, Si SiC and Fe−Cr−Al are 88.35%, 94.69%, 74.55%, 90.76%, respectively. This suggests that the Si-coated cladding has the best crack tolerance in the four materials. The crack tolerance of Cr and Fe−Cr−Al is also good. However, the SiC-coated cladding has the worst performance in the crack tolerance. If the crack length in SiC coating exceeds three quarters of the coating thickness, the cladding will fail.

3.2. Crack propagation along the radial direction

When the length of coating crack exceeds the critical length mentioned in 3.1, the cladding will fail. However, if the crack length is within the allowable range, the crack may still propagate along the *r*-direction to the cladding. This phenomenon will also result in the cladding failure. We calculated the energy release rate when the crack propagated along the *r*-direction, as shown in Fig. 9:

Compared the black lines in Fig. 9 with the fracture experiment results of Cr-coated Zircaloy cladding in Ref. [11], the relation between energy release rate and crack length is similar. Therefore, for the other coating materials, the results in this paper are credible. However, because of the difference mechanical properties of coating material, there are differences in specific values. For the same coating thickness, energy release rates of four coating materials were different. The energy release rate of SiC-coated cladding was at the highest level because of its high Young's modulus. Energy release rates of Cr and Fe−Cr−Al were similar and Si had the lowest level. For the same material, there is an approximately quadratic relationship between the crack length and the energy release rate when the crack propagates along the *r*-direction. Considering the stress distribution near the crack is continuous, if the crack starts to propagate along the *r*-direction, it will not stop until the crack tip reaches the cladding and result in the cladding failure. Meanwhile, the propagation speed of crack increases with the increase of crack length. Considering the different fracture toughness of Cr, Si, SiC and Fe−Cr−Al in Table 1, it is important to find out the critical crack length at which the crack propagates along the *r*-direction, as shown in Fig. 10:

The fracture toughness of material varies within a range. Therefore, the crack lengths have been divided into three regions. The bases of the division of different zones are shown in the
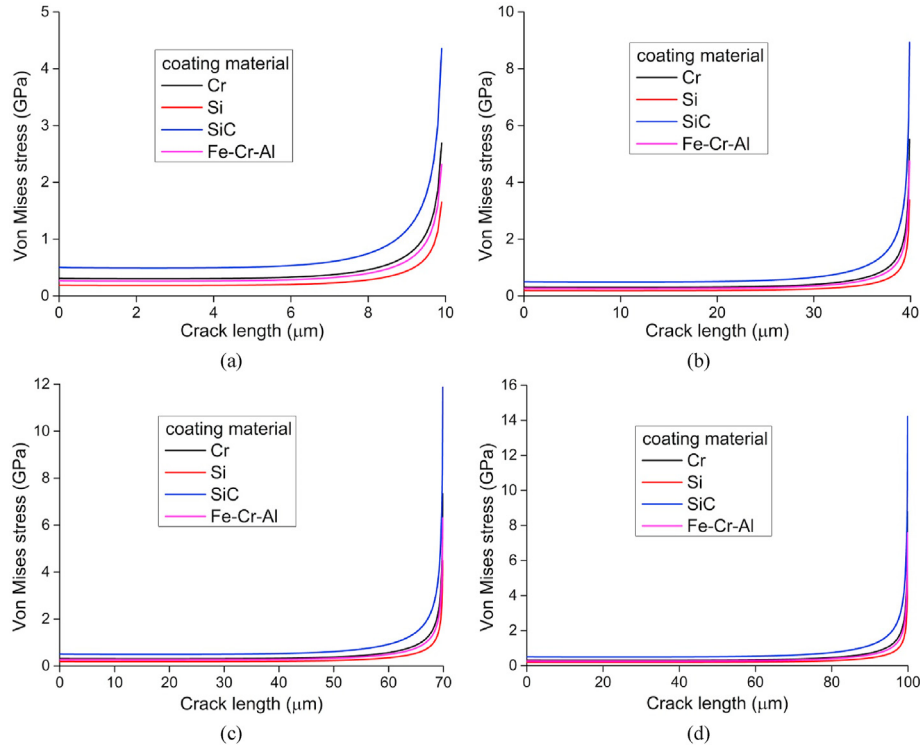
Fig. 7. The von Mises stress at the interface between coating and cladding at different coating thicknesses: (a) 10 μm, (b) 40 μm, (c) 70 μm, (d) 100 μm.
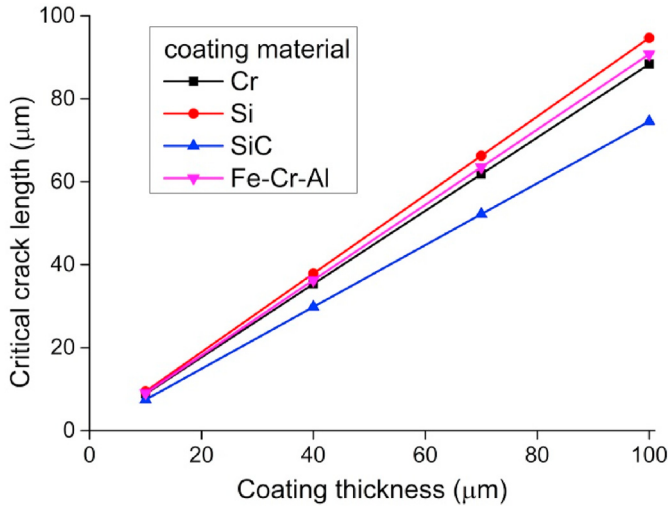

Fig. 8. The critical crack length with different coating material and thickness.

following equation:

$$
\begin{cases}
danger\ zone, & G_r > \Gamma_{upper}\ or\ a > a_c \\
safety\ zone, & G_r < \Gamma_{lower}\ and\ a < a_c \\
discussion\ zone, & \Gamma_{lower} < G_r < \Gamma_{upper}\ and\ a < a_c
\end{cases} \quad (9)
$$

Where Γ_{upper} and Γ_{lower} are the upper and lower bound of the fracture toughness of different materials (kJ/m^2), respectively, a_c is the critical crack length mentioned in 3.1 (m).

The safety zone is the region that the energy release rate is lower than the lower bound of the fracture toughness. The crack is stable and will not continue to propagate. The coating thickness of surface-coated Zircaloy cladding should be designed within the safety zone, if possible. The danger zone is the region that meets either of the

follow conditions. First, the energy release rate is higher than the upper bound of the fracture toughness. That means, the crack is unstable and must propagate to the cladding. Second, the initial crack length is longer than the critical length. If the crack length is in the danger zone, the cladding will fail because of the crack propagation or excessive stress level. And the probability of cladding failure is 1. The discussion zone is the region that the initial crack length is between the upper and lower bound. It is difficult to determine whether the crack can propagate or not. If the coating thickness is designed within the discussion zone, it is necessary to determine whether it is feasible according to the actual situation.

It can be seen from Fig. 10 that differences among the zones for different materials are considerable. This is because of the different properties, such as Young's modulus, Poisson's rate, fracture toughness, of different materials. Si and SiC are not suitable as the coating material if we have a higher requirement for fracture resistance. Though they have excellent performance in statics analysis [13,33]. When the coating is thin, such as 10 μm, the allowable initial crack lengths of Si-coated and SiC-coated cladding are approximately fifty percent of the coating thickness. It is not a good performance compared with the other two coating materials. With the increase of coating thickness, crack tolerances of Si and SiC decrease. When the coating thickness is 100 μm, the allowable crack length is only about ten percent of the coating thickness.

Cr and Fe−Cr−Al have relatively better crack resistance. When the coating is thin, the crack will not propagate and the cladding failure is caused by the stress concentration near the crack tip (Fig. 10(a)). When the coating is thick, such as thicker than 50 μm, the crack tolerance of Cr-coated cladding decreases obviously. However, Fe−Cr−Al-coated cladding still keeps a high allowable crack length which is more than eighty percent of the coating thickness (Fig. 10(c), (d)).

Therefore, if the coating is thin, Cr and Fe−Cr−Al are suitable coating materials. If the coating is relatively thick and the power of fuel element is high, which may result in a high stress level in the
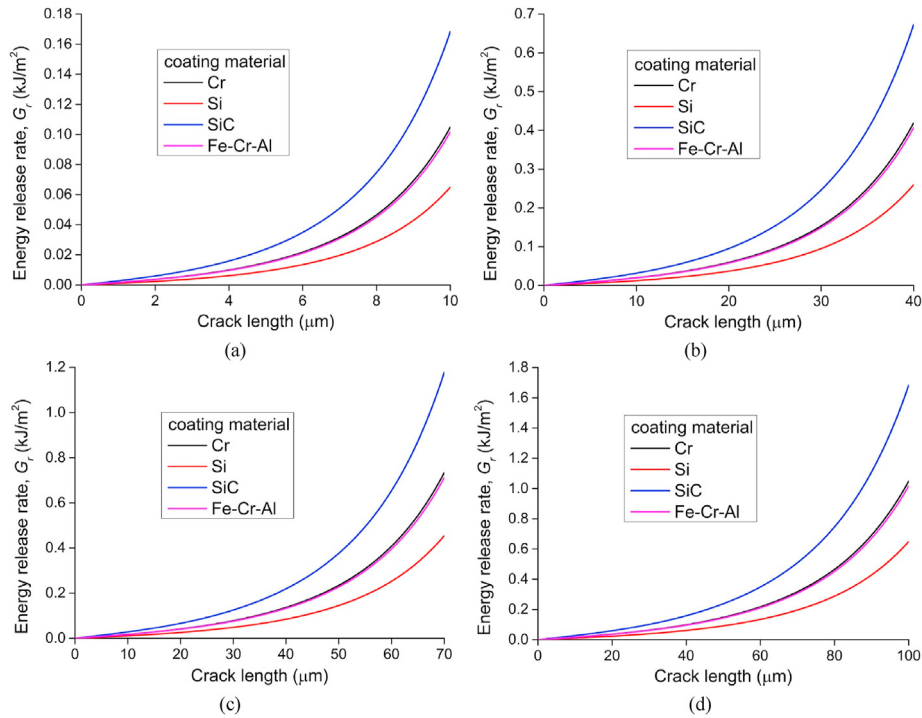
Fig. 9. The energy release rate when the crack propagates along the *r*-direction at different coating thicknesses: (a) 10 μm, (b) 40 μm, (c) 70 μm, (d) 100 μm.
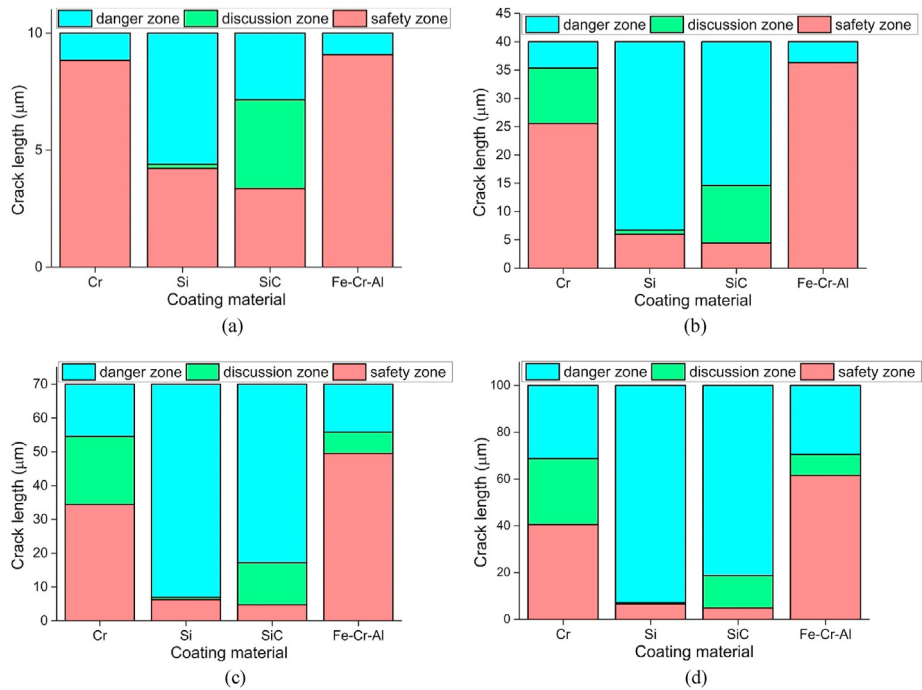

Fig. 10. The effect of crack length on crack propagation along the *r*-direction at different coating thicknesses: (a) 10 μm, (b) 40 μm, (c) 70 μm, (d) 100 μm.

coating, Fe–Cr–Al-coated cladding is the best choice for keeping component integrity. Considering the excellent performance in statics analysis, Si-coated and SiC-coated claddings can be used in the low power reactor where the develop probability of crack is low.

3.3. Crack propagation along the axial direction

A crack channel can be formed in the coating because of the crack propagation along the *z*-direction. We assumed that the axial crack length was the same as the coating thickness. This assumption had little effect on results because of the large difference between coating thickness and cladding length. Also, the energy release rate was calculated to determine whether the crack propagated along the *z*-direction or not, as shown in Fig. 11:

Until now, experiments for the crack propagation along the axial direction in surface-coated Zircaloy cladding do not seem to exist in previous investigations. Compared with the finite element analysis of Cr-coated Zircaloy cladding in Ref. [10], results in this paper are
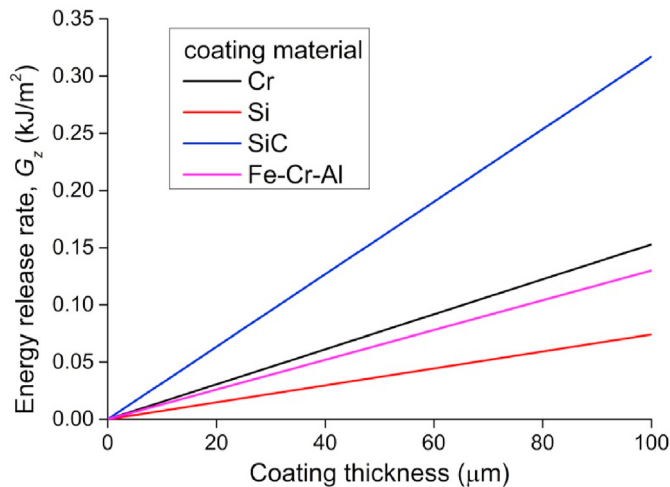
Fig. 11. The energy release rate when the crack propagates along the *z*-direction.

credible. It can be seen from Fig. 11 that the energy release rate when the crack propagates along the *z*-direction varies approximately linear with the coating thickness. Therefore, if the coating thickness exceeds the critical value and the coating has an initial crack, this crack can keep propagating until a complete crack channel is formed in the coating. This crack channel can destroy the integrity of the coating and result in a spalling, even the failure, of the coating. The propagation of the crack under different coating thicknesses has been summarized, as shown in Fig. 12:

The meaning of each zone in Fig. 12 is the same as Fig. 10. Bases of the division of different zones are the same as equation (9) but G_r should be changed into G_z. It can be seen that crack channels along the axial direction are formed in Si-coated and SiC-coated claddings if the coating is thicker than about 10 μm, 20 μm, respectively. This greatly limits the optional range of coating thickness. Considering conclusions in 3.2, the allowable crack length of Si-coated and SiC-coated claddings should not exceed fifty percent of the coating thickness. It is a high requirement in the manufacture of the coating. However, Cr and Fe–Cr–Al have excellent performance in preventing the formation of crack channel. When the coating thickness is less than about 60 μm, no crack channel is formed in the Cr-coated or Fe–Cr–Al-coated cladding unless the crack length exceeds the critical length mentioned in 3.2. When the coating is thicker than 60 μm, the Fe–Cr–Al-coated cladding is still in the safety zone but
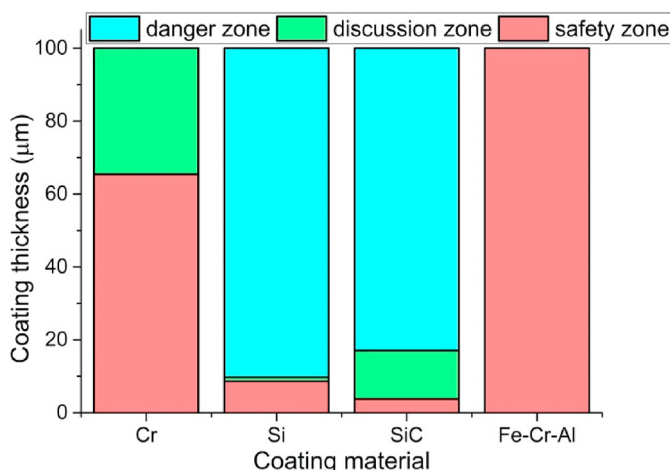
whether the crack channel will be formed in the Cr-coated cladding or not depends on the actual situation. Therefore, the conclusion is the same as 3.2 that if the coating is thin, Cr and Fe–Cr–Al are suitable coating materials. If the coating is thick, Fe–Cr–Al is the best choice for the coating material.

Considering the fact that Cr-coated cladding has the widest investigation and mature manufacturing methods of all surface-coated Zircaloy cladding [9,12], the choice of Cr-coated cladding is more secure under the same condition. Therefore, when the coating is thin, Cr-coated cladding is a better choice than Fe–Cr–Al-coated cladding.

4. Conclusions

In this paper, the authors established the model of surface-coated Zircaloy cladding which coating materials are Cr, Si, SiC, Fe–Cr–Al, respectively. The mechanical behaviors of crack in the coating, such as the stress field at crack tip, crack propagation along the radial and axial directions, have been investigated. The results indicate that the stress field at crack tip in the coating may result in the failure of cladding. There is a critical crack length in the coating which determines whether the cladding can fail caused by the stress field at crack tip or not. Different coating materials have different critical crack lengths. In our investigation, the critical crack lengths of Cr, Si and Fe–Cr–Al are about ninety percent of the coating thickness, which is an excellent value of the crack tolerance. However, the critical crack length of SiC-coated cladding is less than three quarters of the coating thickness.

By analyzing conditions of different coating crack propagations along the radial and axial directions and considering the universality of engineering manufacturing, the application range of different coating materials has been concluded. Cr-coated cladding is suitable for the coating which is thinner than 40 μm. Fe–Cr–Al-coated cladding can keep the integrity of the cladding maximally when the coating is thicker than 40 μm. Therefore, if the coating is thicker than 40 μm, Fe–Cr–Al is ideal coating material. However, Si-coated and SiC-coated claddings have poor crack tolerance. They can only be used in low power reactor, which has a low stress level and develop probability of the crack. These conclusions can provide reference for related experiments in the future and predict experimental results.

The results in our investigation showed that the crack propagation along the axial direction will lead to a crack channel throughout the coating, which may result in a local spalling of the coating. A local spalling is a phenomenon that the crack propagation is perpendicular to the radial direction and result in a detachment of a small piece of the coating. The mechanism of coating spalling is important and should be investigated in following works. If the plane of crack is not perpendicular to the axial direction, the crack propagation becomes a three-dimensional problem and the axial stress need to be considered. Furthermore, because of the lack of experiment data, the crack propagation experimental analysis of surface-coated Zircaloy cladding which has different coating materials is also important.

Declaration of competing interest

The authors declare that they have no known competing financial interests or personal relationships that could have appeared to influence the work reported in this paper.

Fig. 12. The effect of coating thickness on crack propagation along the *z*-direction.

References

[1] B.W. Qiu, J. Wang, Y.B. Deng, M.J. Wang, Y.W. Wu, S.Z. Qiu, A review on thermohydraulic and mechanical-physical properties of SiC, FeCrAl and Ti3SiC2 for ATF cladding, Nucl. Eng. Technol. 52 (2020) 1−13.

[2] H.G. Kim, I.H. Kim, J.Y. Park, Y.H. Koo, Application of coating technology on zirconium-based alloy to decrease high-temperature oxidation, in: ASTM Special Technical Publication, 2015, pp. 346−369.

[3] J. Wang, H. Yeom, P. Humrickhouse, K. Sridharan, M. Corradini, Effectiveness of Cr-coated Zr-alloy clad in delaying fuel degradation for a PWR during a station blackout event, Nucl. Technol. 206 (2019) 467−477.

[4] Y. Lee, J.I. Lee, H.C. No, Mechanical analysis of surface-coated zircaloy cladding, Nucl. Eng. Technol. 49 (2017) 1031−1043.

[5] M. Wagih, B. Spencer, J. Hales, K. Shirvan, Fuel performance of chromium-coated zirconium alloy and silicon carbide accident tolerant fuel claddings, Ann. Nucl. Energy 120 (2018) 304−318.

[6] J. Krejčí, J. Kabátová, F. Manoch, J. Kočí, L. Cvrček, J. Málek, S. Krum, P. Šutta, P. Bublíková, P. Halodová, H.K. Namburi, M. Ševeček, Development and testing of multicomponent fuel cladding with enhanced accidental performance, Nucl. Eng. Technol. 52 (2020) 597−609.

[7] T. Dabney, G. Johnson, H. Yeom, B. Maier, J. Walters, K. Sridharan, Experimental evaluation of cold spray FeCrAl alloys coated zirconium-alloy for potential accident tolerant fuel cladding, Nucl. Mater. Energy 21 (2019) 10.

[8] M. Kennas, H. Kim, J.G. Gigax, T. Wang, B.R. Maier, H. Yeom, G.O. Johnson, T. Dabney, K. Sridharan, K.L. Peddicord, L. Shao, Radiation response of FeCrAl-coated zircaloy-4, J. Nucl. Mater. 536 (2020) 152175.

[9] H.G. Kim, I.H. Kim, Y.I. Jung, D.J. Park, J.Y. Park, Y.H. Koo, Adhesion property and high-temperature oxidation behavior of Cr-coated Zircaloy-4 cladding tube prepared by 3D laser coating, J. Nucl. Mater. 465 (2015) 531−539.

[10] K. Hong, J.R. Barber, M.D. Thouless, W. Lu, Cracking of Cr-coated accident-tolerant fuel during normal operation and under power-ramping conditions, Nucl. Eng. Des. 353 (2019) 110275.

[11] D.C. Roache, A. Jarama, C.H. Bumgardner, F.M. Heim, J. Walters, J. Romero, B. Maier, X. Li, Unveiling damage mechanisms of chromium-coated zirconium-based fuel claddings by coupling digital image correlation and acoustic emission, Mater. Sci. Eng., A 774 (2020) 138850.

[12] K.A. Terrani, Accident tolerant fuel cladding development: Promise, status, and challenges, J. Nucl. Mater. 501 (2018) 13−30.

[13] Y. Lee, M.S. Kazimi, A structural model for multi-layered ceramic cylinders and its application to silicon carbide cladding of light water reactor fuel, J. Nucl. Mater. 458 (2015) 87−105.

[14] D.R. Olander, Fundamental aspects of nuclear reactor fuel element, in: Department of Nuclear Engineering, California University, 1976. Berkeley, USA.

[15] L. China, Nuclear Power Engineering Co., Suzhou Nuclear Power Research Institute, Nuclear Power Plant Metal Materials Manual, China Electric Power Press, Beijing, 2017.

[16] G. Simmons, Single crystal elastic constants and calculated aggregate Progress, J. Grad. Res. Cent. 34 (1965) 273.

[17] A. Masolin, P.O. Bouchard, R. Martini, M. Bernacki, Thermo-mechanical and fracture properties in single-crystal silicon, J. Mater. Sci. 48 (2013) 979−988.

[18] L.L. Snead, T. Nozawa, Y. Katoh, T.S. Byun, S. Kondo, D.A. Petti, Handbook of SiC properties for fuel performance modeling, J. Nucl. Mater. 371 (2007) 329−377.

[19] K.A. Terrani, S.J. Zinkle, L.L. Snead, Advanced oxidation-resistant iron-based alloys for LWR fuel cladding, J. Nucl. Mater. 448 (2014) 420−435.

[20] U. Holzwarth, H. Stamm, Mechanical and thermomechanical properties of commercially pure chromium and chromium alloys, J. Nucl. Mater. 300 (2002) 161−177.

[21] K.E. Petersen, Silicon as a mechanical material, Proc. IEEE 70 (1982) 420−457.

[22] B.Q. Yang, K. Zhang, G.N. Chen, G.X. Luo, J.H. Xiao, Measurement of fracture toughness and interfacial shear strength of hard and brittle Cr coating on ductile steel substrate, Surf. Eng. 24 (2008) 332−336.

[23] F. Ebrahimi, L. Kalwani, Fracture anisotropy in silicon single crystal, Mater. Sci. Eng. A-Struct. Mater. Prop. Microstruct. Process. 268 (1999) 116−126.

[24] S. Nogami, A. Hasegawa, L.L. Snead, Indentation fracture toughness of neutron irradiated silicon carbide, J. Nucl. Mater. 307 (2002) 1163−1167.

[25] K.H. Park, S. Kondo, Y. Katoh, A. Kohyama, Mechanical properties of beta-SiC after Si- and dual Si plus He-ion irradiation at various temperatures, Fusion Sci. Technol. 44 (2003) 455−459.

[26] M.N. Gussev, K.G. Field, Y. Yamamoto, Design, properties, and weldability of advanced oxidation-resistant FeCrAl alloys, Mater. Des. 129 (2017) 227−238.

[27] R.L. Williamson, Enhancing the ABAQUS thermomechanics code to simulate multipellet steady and transient LWR fuel rod behavior, J. Nucl. Mater. 415 (2011) 74−83.

[28] G.R. Irwin, R. de Wit, A summary of fracture mechanics concepts, J. Test. Eval. 11 (1983) 56−65.

[29] H. Tada, P.C. Paris, G.R. Irwin, Stress Analysis of Cracks Handbook, 3 ed., American Society of Mechanical Engineers, United States, 2000.

[30] J.L. Beuth Jr., Cracking of thin bonded films in residual tension, Int. J. Solid Struct. 29 (1992) 1657−1675.

[31] D.B. Bogy, Edge-bonded dissimilar orthogonal elastic wedges under normal and shear loading, J. Appl. Mech. 35 (1968) 460−466.

[32] J. Dundurs, Discussion on "Edge-bonded dissimilar orthogonal elastic wedges under normal and shear loading, J. Appl. Mech. 36 (1969) 650−652.

[33] V.A. Avincola, P. Guenoun, K. Shirvan, Mechanical performance of SiC three-layer cladding in PWRs, Nucl. Eng. Des. 310 (2016) 280−294.